# Shape effects on magnetization state transitions in individual 160-nm diameter Permalloy disks

Zhigang Liu* and Richard D. Sydora
*Department of Physics, University of Alberta, Edmonton, Alberta, Canada T6G 2G7*

Mark R. Freeman
*Department of Physics, University of Alberta, Edmonton, Alberta, Canada T6G 2G7*
*and National Institute for Nanotechnology, 11421 Saskatchewan Drive, Edmonton, Alberta, Canada T6G 2M9*

(Received 29 November 2007; revised manuscript received 4 March 2008; published 8 May 2008)

The spin dynamics in individual Permalloy nanodisks has been investigated by using time-resolved magneto-optical Kerr effect microscopy. Transitions between the vortex and quasisingle domain states have been observed by sweeping the applied bias field, and the critical bias fields for triggering vortex annihilation and nucleation have been determined by associated frequency shifts of 5–10 GHz in ferromagnetic resonance. The shape of the nanodisks has to be taken into account in three-dimensional micromagnetic simulations to obtain consistent results for the critical fields when compared to the experiment.

DOI: 10.1103/PhysRevB.77.174410 PACS number(s): 75.75.+a, 75.40.Gb, 75.60.Ej, 76.50.+g

In recent years, remarkable progress has been made in exploring the equilibrium and dynamic properties of small magnetic elements, which is motivated by their applications in magnetic storage technology such as magnetoresistive random access memory.[1,2] Many other applications in spintronics, which rely on the spin degree of freedom in electronic devices, are also based on nanoscale magnetic systems.[3] The demands for a high storage density, a fast processing speed, and low energy consumption have brought together knowledge and techniques to spur the subfield of nanomagnetism.[4,5]

One of the most interesting and useful features of nanomagnets is their different ground states under certain conditions, which can form a technical basis for encoding information. In general, the ground states result from the competition of all terms contributing to the Hamiltonian of the system that leads to a minimization of the total energy. The vortex and quasisingle domain states are the two main configurations in a ferromagnetic nanodisk. The demagnetization field plays the key role in favoring the vortex configuration in low external fields, with the size of the vortex core determined by competition with the exchange interaction. By using methods such as energy functional theory, variational theory, and micromagnetic simulation, a variety of analytical and computational studies were reported to elucidate the dynamics of the two states and the transitions between them.[6–8] However, a potential problem arises because most theories and calculations have modeled the nanodisk as a perfect cylinder (with a rectangular cross section from the side view), while with current fabrication technologies, it is difficult to approximate the samples in that way. In this paper, we show that the shape of the nanodisks significantly affects the vortex-to-quasisingle domain state transitions.

Many experimental studies on nanomagnets measure the total signals from a large number of elements in two-dimensional arrays, self-assembled composite, etc.[9–11] Uncertainties due to size and shape variation, and in some cases dipolar coupling within arrays, can give unclear information concerning the behavior of state transitions. Experiments on individual nanomagnets below 200 nm have recently begun to be reported,[12–14] which focused on either the vortex state or the quasisingle domain state. In this work, we report on observations for both of these states, which were measured on individual Permalloy nanodisks with a diameter of about 160 nm. Time-resolved magneto-optical Kerr effect microscopy (TRMOKE) was used to monitor the small-angle perturbation response of the magnetization (spin wave dynamics) in the nanodisks. A bias magnetic field was applied parallel to the disk plane, and a short magnetic pulse was used to excite the spin waves in the nanodisks. The resonant frequency is a sensitive fingerprint of the equilibrium magnetic configuration, providing insight into the details of hysteresis in small structures complimentary to that obtained by magnetic force microscopy, Lorentz microscopy, or electron holography.

The Permalloy disks were fabricated on sapphire substrates by standard electron beam lithography (EBL), metallization, and lift-off procedures. Then, photolithography was performed to fabricate gold transmission lines near the Permalloy disks for excitation. A micrograph of a sample is shown in Fig. 1(a), wherein the pump-probe measurement scheme is also sketched. The experimental details, including the fast pulse generation using a GaAs photoconductive switch, are described in previous work[15–17] and remain similar here. The pulse field has both in-plane and out-of-plane components since the disks with good signals have to be very close to the transmission lines; the peak amplitude is in the range of $10^3$ A/m, as can be estimated by sampling the current with a fast oscilloscope and then calculating the field with the Biot–Savart law. Scanning electron microscope (SEM) images of the nanodisks are shown in Figs. 1(b) and 1(c). The tops of the disks are somewhat domed as a result of shadowing during deposition through the double-layer resist openings. The deposited thickness was measured as 30 nm in a witness film. In addition, there is an edge roughness on the 10-nm scale that arises from the granularity of the film. The distance between neighboring disks is about 900 nm (>5 disk diameters), allowing dipolar interactions to be neglected, and the probing laser was focused on a single disk (spot size of <700 nm).

The time traces in Fig. 2 show the characteristic time-domain response of the out-of-plane component of magneti-

 

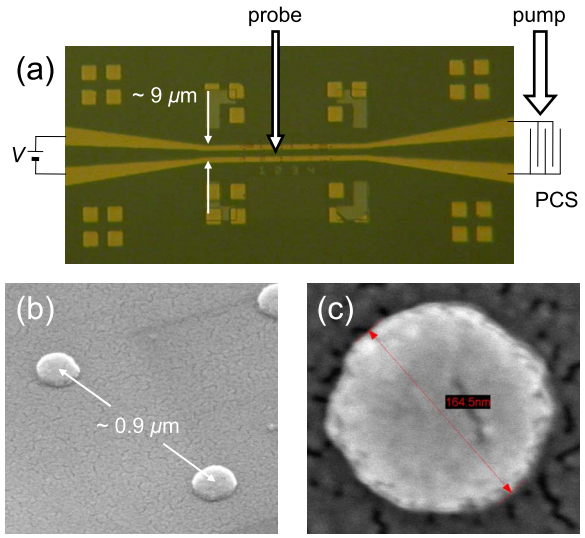


FIG. 1. (Color online) (a) Micrograph of the sample showing the gold transmission lines (yellow) and the Permalloy patterns (light green); the visible Permalloy structures are useful for alignment and for locating the nanomagnets. The circuit connections for TRMOKE measurement are also sketched, with the photoconductive switch (PCS) on one end of the transmission lines and a bias voltage on the other end ($V$=10–15 V). (b) SEM image of the Permalloy disks captured at a 45° tilted angle. (c) SEM top view of one of the disks shown in (b); its diameter is displayed by the SEM software, which reads "164.5 nm."

zation ($M_z$) to the pulsed excitation. The disk is in a single-domain state when sufficiently saturated by strong bias fields such as $H_0$=95.5 kA/m in Fig. 2(a). It should be noted that there is no extrinsic dephasing due to averaging the signals from an ensemble of magnets. The decay time constant $1.8 \pm 0.3$ ns reasonably agrees with those measured in thin films or bulk Permalloy. At very small bias fields [$H_0$ =0.24 kA/m in Fig. 2(b)], the disk is always in a vortex

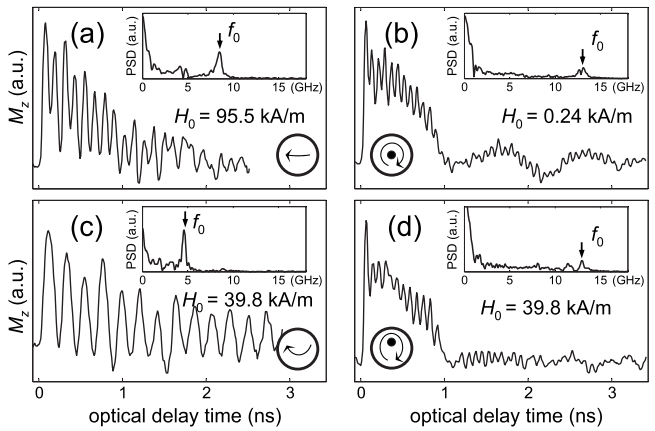


FIG. 2. [(a)–(d)] Evolutions of $M_z$ as a function of the pump-probe optical delay time measured under different bias fields and ground states (quasisingle domain or vortex), as illustrated by the cartoons in each panel. The power spectral densities (PSD) of the time traces are shown by the insets, with the arrows marking the characteristic frequency $f_0$ as the indicator for state transitions discussed in the text.

state, exhibiting much higher modal frequencies than the uniformly magnetized state. For intermediate bias fields, distorted versions of both the single domain and vortex states can be stable, depending upon the magnetic history. Figures 2(c) and 2(d) show the measurements for $H_0$=39.8 kA/m. In this case, the magnetization is only partially saturated to form a quasisingle domain or $C$ state, as illustrated by the schematic insets. The bending of the "$C$" shape increases with decreasing bias field until at the nucleation field strength $H_{nu}$, the magnetization will close around a core and generate a vortex state. At low bias fields, the vortex core stays near the center of the disk [inset of Fig. 2(b)]. The core is pushed toward the edge by increasing $H_0$ until it is expelled when it reaches the disk edge at the annihilation field strength $H_{an}$.

These transitions are identifiable from the measured wave forms and most conveniently by their frequencies, which are obtained by Fourier transformation. For the quasisingle domain state, the relatively uniform oscillation is the only significant mode in the spectra [see the insets of Figs. 2(c) and 2(e)], and the frequency $f_0$ was given by Guslienko *et al.*[18] by using a modified Kittel's formula

$$f_0 = \frac{\gamma_0}{2\pi}\sqrt{H_0^2 + H_0 M_s[1 - 3F(\beta)]}, \tag{1}$$

where $M_s$ is the saturation magnetization, $\gamma_0$ is the gyromagnetic ratio, and $F(\beta)$ is the effective demagnetizing factor for a cylinder with $\beta$ equal to the thickness-to-radius ratio. For the vortex state, the high-frequency dynamics[19] exhibits relatively complicated profiles in the frequency domain, and $f_0$ is chosen as the frequency of the primary mode [with the highest spectral density; see the insets of Figs. 2(b) and 2(d)]; the observed secondary modes will be discussed below.

The variation in $f_0$ as a function of $H_0$ are plotted as squares in Fig. 3(a). The quasisingle domain state frequencies closely follow the modified Kittel's formula (gray curve) except for the low-$H_0$ region in which the $C$-shape configuration leads to significantly lower frequencies than those predicted by assuming an ideal uniform state. When $H_0$ is lowered below 29 kA/m, there is a frequency jump of ~10 GHz as a result of a single domain to vortex state transition (vortex nucleation). If the applied field amplitude is increased while in the vortex state, the resonance frequency is maintained at ~13 GHz, which is characteristic of Permalloy disks at this aspect ratio,[20–22] until $H_0$ is larger than ~40 kA/m, whereupon $f_0$ drops to ~11 GHz. The lower frequency is characteristic of a thinner disk and suggests that the vortex core is affected by the sloping disk edge. An abrupt frequency drop of ~5 GHz is observed when $H_0$ increases to ~68 kA/m and registers the vortex to quasisingle domain transition (vortex annihilation). The measured nucleation and annihilation fields corresponded within 1 kA/m for repeated bias field sweeps and had variations of ~1.6 kA/m for different disks.

In a single sweeping cycle, it was observed that a transition can be spontaneously triggered when the bias field was *fixed* in the critical region. Figure 4(a) shows an example when $H_0$ was fixed at 67.4 kA/m. Before the moment recorded for the annihilation [marked by the arrow in Fig.

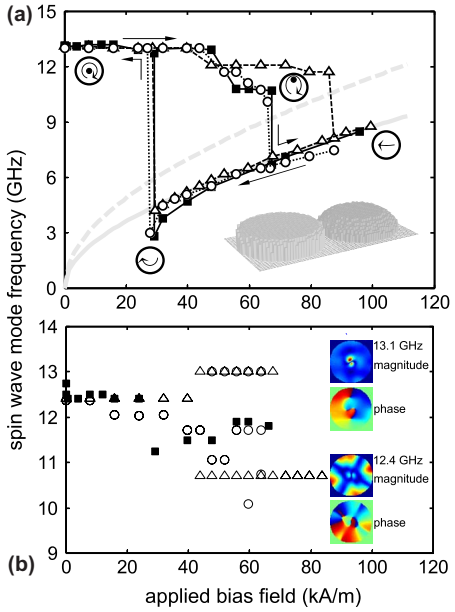


FIG. 3. (Color online) Spin wave frequencies of the Permalloy disk. The measured data are plotted by squares, and the simulated results obtained by using the domed cylinder model and the flat cylinder model are plotted as circles and triangles, respectively. (a) Hysteresis behavior of the primary modal frequency ($f_0$) as a function of the bias field ($H_0$), with the arrows indicating the sweep direction of the bias field. The representative magnetization states are also sketched. The inset 3D cartoon shows the shapes of the two models. The gray curve is calculated based on Eq. (1) (for our samples, $\beta=0.375$ and $F(\beta)\approx 0.1537$, see Ref. 18 for details); the gray dashed curve gives a reference calculation based on the unmodified Kittel's formula, i.e., $F(\beta)=0$. (b) Frequencies of the secondary modes in the vortex states. The insets show the simulated magnitude and phase distributions of the primary mode [13.1 GHz, see (a)] and the secondary mode (12.4 GHz) when $H_0=0$. The color bars (not shown) are scaled by the maximum and minimum of individual maps.

4(a)], the vortex state was sustained for more than 10 min (each 12 ps delay time step in the pump-probe measurement took about 4 s in real time). A similar behavior was also observed for the vortex nucleation process when $H_0$ was fixed at 29.1 kA/m [Fig. 4(b)]; the quasisingle domain state had survived for more than 10 min before the vortex appeared. These facts demonstrate that when measuring a single nanomagnet, its magnetic properties (not only $f_0$ but also the magnetization $M$, the susceptibility $\chi$, and so on) in a single bias field sweep should show an effectively discontinuous change when a state transition occurs. In contrast, if conventional hysteresis data ($M$ as a function of $H_0$) were obtained by averaging over an array,[9,23,24] these state transitions would appear to be gradually completed within a small range of $H_0$, mostly due to the variation of shape and size within the array, and hence cannot grasp the details revealed in the present work. Similarly, in time-resolved measurements, the spontaneous switching events can only be observed by measuring individual nanomagnets; the transition events are stochastic among different disks and would produce incoherent temporal data if many disks were collectively measured.

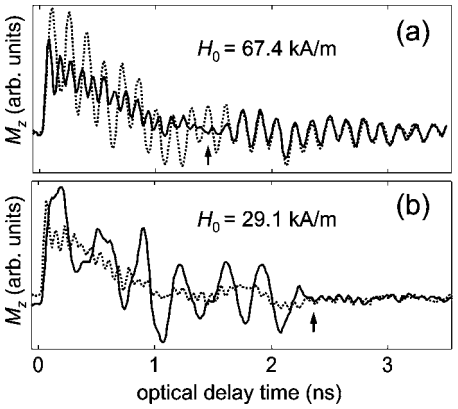


FIG. 4. (a) The solid curve shows the temporal scan of $M_z$ with an abrupt change in the precession behavior, indicating a vortex-to-quasisingle domain transition (marked by the arrow); the dashed curve shows an immediately followed scan to confirm the disk was already in the quasisingle domain state. The bias field was fixed at 67.4 kA/m during the scans. (b) Similar consecutive scans for detecting a quasisingle domain to vortex transition. The bias field was fixed at 29.1 kA/m.

To better understand the observed state transitions and frequency data, micromagnetic simulations were performed based on the Landau–Lifshitz–Gilbert equation.[25] In the calculations, $M_s=8.2\times 10^5$ A/m, $\gamma_0=1.854\times 10^{11}$ s$^{-1}$ T$^{-1}$, and the exchange stiffness coefficient $A=1.0\times 10^{-11}$ J/m. A large Gilbert damping constant $\alpha=1.8$ was used for fast ground state stabilization so that reasonable estimations for $H_{\rm an}$ and $H_{\rm nu}$ can be made. The sweep step for the bias field was 0.8 kA/m near critical fields and was larger for unimportant regions. Then, in accordance to our experimental conditions, the excitation pulse was applied to the system under a finite temperature $T=350$ K (an upper-limit estimation, considering the laser heating) and the relaxation dynamics were simulated with the real damping constant $\alpha=0.008$ to test the stability of corresponding states and find more accurate ranges for $H_{\rm an}$ and $H_{\rm nu}$. The corrections due to these perturbations were below 0.8 kA/m. The finite-element discretization was done on a $64\times 64\times 8$ rectangular grid,[26] and two shapes for the nanodisk were used (see the inset of Fig. 3); a flat-topped cylinder similar to those adopted by the aforementioned theoretical and computational work and a more realistic "domed" cylinder to qualitatively model the actual samples are shown in Figs. 1(b) and 1(c). For both models, granular defects of 5–10 nm in size were randomly generated at the edges.

Simulation results for the $f_0$-$H_0$ curves are plotted in Fig. 3(a) (circles for the domed cylinder model and triangles for the flat cylinder model) to compare to the measurements. Despite small discrepancies in the frequencies, the main features are reproduced reasonably well, such as the low-$H_0$ deviation from the modified Kittel's formula due to the $C$ state and the small frequency drop when $H_0>47.8$ kA/m. Concerning the state transitions, the domed model fits the experiments much better than the flat model. A significant difference occurs for the vortex annihilation field; the flat cylinder model gives $H_{\rm an}\approx 87.5$ kA/m, which reasonably agrees with the results in Ref. 6, while the domed cylinder

model leads to a much smaller $H_{an} \approx 66.9$ kA/m, which is very close to the measured value. The process can be easily visualized through the simulated spatial images, in which the vortex core can reach the round-corner surface at a relatively low bias field. The upper portion of the core will then be geometrically destabilized by the curved shape, resulting in the earlier annihilation.

It is also interesting to investigate the distributions of the vortex-state modes, which, under a specific $H_0$, exhibit certain secondary peaks near the primary mode with comparable intensities. The measured and simulated results for the secondary modes are plotted in Fig. 3(b). These modes, together with the primary modes shown in Fig. 3(a), appear to fill in discrete frequency levels when the bias field increases. This type of mode distribution was intensively investigated in larger disks wherein spatially resolved measurements were possible.[20,21] The high-frequency vortex state oscillations can be quantized in radial and azimuthal directions by the number pair $(n,m)$, which indexes the orders of specific spin wave modes. This picture does not cleanly map onto our small radius samples with imperfect circular symmetry, where a symmetrical, "uniform" oscillation (0, 0) is no longer an eigenmode of the disk. No radial nodes are found in simulations, suggesting that $n=0$ under the present excitation conditions. The multiple peaks in the range of 10–13 GHz exhibit stationary phase as well as left- and right-phase circulation patterns that can only approximately be identified with different azimuthal indices $m$. The insets of Fig. 3(b) present the simulated magnitude and phase distributions of the 13.1 GHz (primary) and the 12.4 GHz (secondary) modes when $H_0=0$. The asymmetry of the structure selects particular nonuniform modes. The azimuthal distribution is not uniform for the primary mode, although no nodes are visible. In addition, this mode is stationary after being reconstructed in the time domain by using the method introduced in Ref. 21. The secondary mode, however, shows a clear quantization $(m=4)$ and is rotating counterclockwise.

When the bias field becomes strong enough $(H_0 > 45$ kA/m), the primary mode shifts to lower frequencies. This trend indicates an increasing influence of the thinner edge of the disk as the vortex is driven far off center. The declining primary mode frequency is more accurately described by the domed cylinder model than the flat cylinder model [see the data between 45 and 65 kA/m in Fig. 3(a)].

For the uniform-to-vortex state transition with decreasing field (vortex nucleation), the simulations show that the critical bias field does *not* have significant dependence on the models with different shapes. The $H_{nu}$ values determined by both models are consistent with the measurements [Fig. 3(a)] and also agree with the results from other simulation work.[6] The nucleation process simulated by the two models can be compared by using the images presented in Fig. 5 (for faster execution, we used $\alpha=1.8$ and $T=0$ K in these calculations, so the evolution is not on real time scales). The bias field was set slightly above the critical range to fully stabilize the quasisingle domain state [Figs. 5(a1) and 5(b1)] so that a subsequent 0.8 kA/m step down can trigger the nucleation process. We found that in both models, the vortex core emerges from the bottom edge of the nanodisk (although for the flat cylinder model, the bottom and top sides are symmetric in geometry), while the spins near the top of the nanodisk still remain in quasisingle domain state [Figs. 5(a2) and 5(b2)]. Note that in these two cases, the spins in the nucleation volume precess out of the disk plane before forming a vortex core penetrating the entire thickness. The shape at the top of the disk does not affect the early stage of vortex nucleation near the bottom, and the nucleation fields produced by the two models differ by just 1.6 kA/m, which is much smaller than the discrepancy for the annihilation fields. After the nucleation, the vortex core moves from the edge to its equilibrium location near the disk center, and its height increases when passing across the edge region [Figs. 5(b3) and 5(b5)].

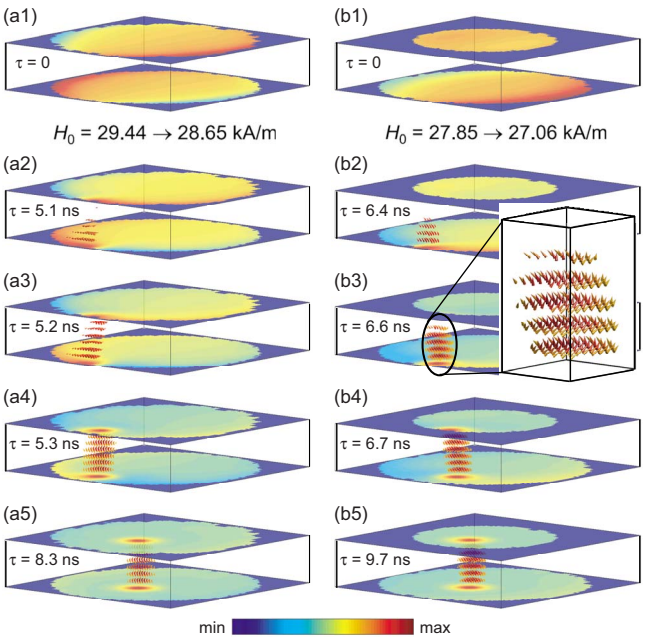


FIG. 5. (Color online) The evolution of magnetization configuration in the vortex nucleation process as simulated by the flat cylinder model [(a1)–(a5)] and the domed cylinder model [(b1)–(b5)]. The disks are stabilized into equilibrium with $H_0=29.44$ kA/m (a1) and 27.85 kA/m (b1), respectively. Then, the bias fields decrease to 28.65 and 27.06 kA/m, respectively, to trigger the nucleation, representative snapshots are recorded in (a2)–(a5) and (b2)–(b5). The $\tau$ values are the "effective" time in the simulations with a large damping constant $\alpha=1.8$, so these snapshots do not reflect the real time points (in real time, the evolutions would be much slower). In each frame, the intensity of $M_z$ at the top and bottom layers of the 3D models are shown by the colored surfaces; the color bar shows a fixed minimum value (−1, assigned for cells outside the magnetic disk) and different maximum values for different frames. The small cones between the two surfaces represent the spins in the 3D models that are within the vortex core (the criterion $\boldsymbol{M}$ being at least 25° off the disk plane); the colors of these cones are also scaled with $M_z$. For clarity, a zoom-in view of the vortex core is presented aside (b3).

To summarize, we have measured the time-resolved magnetic dynamics in individual Permalloy disks of 160 nm diameter. The fundamental mode frequencies of the nanodisk exhibit a distinct hysteresis behavior as a function of the in-plane bias field, and the critical fields for triggering the vortex annihilation and nucleation processes have been

determined. The realistic shape of the nanodisk has to be considered in micromagnetic simulations to explain the measured critical fields. By modifying the shape of the nanodisk, it would be possible to control the annihilation field over a considerable range while keeping the nucleation field unchanged, which could be a useful feature for applications.

The methods described in the present work can be applied to more general nanomagnets, such as rings, squares, or multilayer elements. Issues on the dynamic transition behavior and critical bias fields can be analogously addressed. These investigations may benefit a variety of nanoscale technologies such as magnetic quantum cellular automata[27] that utilize the magnetization state transitions to store and process information.

We thank Hue Nguyen for help with EBL fabrication in the NanoFab of the University of Alberta. This work was supported by NSERC, *i*CORE, CIFAR, and CRC.

*zliu2@ucsc.edu

[1] *Ultrathin Magnetic Structures IV, Applications of Nanomagnetism*, edited by B. Heinrich and J. A. C. Bland (Springer, New York, 2005).
[2] J. Åkerman, Science **308**, 508 (2005).
[3] *Magnetoelectronics*, edited by M. Johnson (Elsevier, Oxford, 2004).
[4] S. D. Bader, Rev. Mod. Phys. **78**, 1 (2006).
[5] C. L. Chien, F. Q. Zhu, and J. G. Zhu, Phys. Today **60**(6), 40 (2007).
[6] K. Yu. Guslienko, V. Novosad, Y. Otani, H. Shima, and K. Fukamichi, Phys. Rev. B **65**, 024414 (2001).
[7] K. Yu. Guslienko, W. Scholz, R. W. Chantrell, and V. Novosad, Phys. Rev. B **71**, 144407 (2005).
[8] R. Zivieri and F. Nizzoli, Phys. Rev. B **71**, 014411 (2005).
[9] R. P. Cowburn, D. K. Koltsov, A. O. Adeyeye, M. E. Welland, and D. M. Tricker, Phys. Rev. Lett. **83**, 1042 (1999).
[10] V. V. Kruglyak, A. Barman, R. J. Hicken, J. R. Childress, and J. A. Katine, J. Appl. Phys. **97**, 10A706 (2005).
[11] A. V. Jausovec, G. Xiong, and R. P. Cowburn, Appl. Phys. Lett. **88**, 052501 (2006).
[12] I. N. Krivorotov, N. C. Emley, J. C. Sankey, S. I. Kiselev, D. C. Ralph, and R. A. Buhrman, Science **307**, 228 (2005).
[13] A. Barman, S. Wang, J. D. Maas, A. R. Hawkins, S. Kwon, A. Liddle, J. Bokor, and H. Schmidt, Nano Lett. **6**, 2939 (2006).
[14] V. S. Pribiag, I. N. Krivorotov, G. D. Fuchs, P. M. Braganca, O. Ozatay, J. C. Sankey, D. C. Ralph, and R. A. Buhrman, Nat. Phys. **3**, 498 (2007).
[15] K. S. Buchanan, X. Zhu, A. Meldrum, and M. R. Freeman, Nano Lett. **5**, 383 (2005).
[16] X. Zhu, Z. Liu, V. Metlushko, P. Grütter, and M. R. Freeman, Phys. Rev. B **71**, 180408(R) (2005).
[17] Z. Liu, F. Giesen, X. Zhu, R. D. Sydora, and M. R. Freeman, Phys. Rev. Lett. **98**, 087201 (2007).
[18] K. Yu. Guslienko and A. N. Slavin, J. Appl. Phys. **87**, 6337 (2000).
[19] The gyrotropic motion of the vortex core, with a low frequency of ~1 GHz, is also visible in some of our measurements, such as, for example, in Fig. 2(b).
[20] J. P. Park and P. A. Crowell, Phys. Rev. Lett. **95**, 167201 (2005).
[21] M. Buess, R. Höllinger, T. Haug, K. Perzlmaier, U. Krey, D. Pescia, M. R. Scheinfein, D. Weiss, and C. H. Back, Phys. Rev. Lett. **93**, 077207 (2004).
[22] C. E. Zaspel, B. A. Ivanov, J. P. Park, and P. A. Crowell, Phys. Rev. B **72**, 024427 (2005).
[23] R. P. Cowburn, J. Phys. D **33**, R1 (2000).
[24] M. Grimsditch, P. Vavassori, V. Novosad, V. Metlushko, H. Shima, Y. Otani, and K. Fukamichi, Phys. Rev. B **65**, 172419 (2002).
[25] We used our own micromagnetics code [Z. Liu, Ph.D. thesis, University of Alberta, 2008].This was benchmarked against M. Scheinfein's, *LLG Micromagnetics Simulator*™ (http://llgmicro.home.mindspring.com/). The code has also been checked by using OOMMF's standard problem No. 4 (http://www.ctcms.nist.gov/~rdm/mumag.org.html).
[26] Test simulations were also performed with $32\times32\times8$ and $64\times64\times16$ grid dimensions, and the results did not show a significant difference.
[27] A. Imre, G. Csaba, L. Ji, A. Orlov, G. H. Bernstein, and W. Porod, Science **311**, 205 (2006).